EUROPEAN ORGANIZATION FOR NUCLEAR RESEARCH
European Laboratory for Particle Physics

Internal Note/Physics
ALICE reference number
ALICE-INT-2006-011 version 1.0

Date of last change
16.08.2006

Topological identification of strange and multi-strange particles with the ALICE detector in Pb-Pb collisions at $\sqrt{sNN}$ = 5.5 TeV

Authors:

Renaud Vernet*, Christian Kuhn*, Jouri Belikov† and Boris Hippolyte*

*IPHC-DRS, Strasbourg, France
†CERN, Geneva, Switzerland

Abstract:
From SPS to RHIC and LHC energies, strangeness production provides one of the major probes for studying strong interacting matter in high energy density conditions and characterizing the Quark Gluon Plasma (QGP). Strange particles can be measured via their weak decay topologies, allowing their identification over a large range of transverse momentum (p_T). Thus, they provide many relevant observables in both i) the soft physics domain, where they represent a key to investigate the global chemical and kinetic freeze- out conditions of the bulk matter as well as its expansion dynamics, and ii) in the hard physics one, where they help to understand jet-quenching phenomena. They also play a crucial role in the intermediate p_T region, being witness of a strong interplay between hard and soft processes.

Topological identification of strange and multi-strange particles with the ALICE detector in Pb-Pb collisions at $\sqrt{s_{NN}} = 5.5$ TeV

Renaud Vernet[*], Christian Kuhn[*], Jouri Belikov[†] and Boris Hippolyte[*]

August 16, 2006

From SPS to RHIC and LHC energies, strangeness production provides one of the major probes for studying strong interacting matter in high energy density conditions and characterizing the Quark Gluon Plasma (QGP). Strange particles can be measured via their weak decay topologies, allowing their identifiation over a large range of transverse momentum (p_T). Thus, they provide many relevant observables in both i) the soft physics domain, where they represent a key to investigate the global chemical and kinetic freeze-out conditions of the bulk matter as well as its expansion dynamics, and ii) in the hard physics one, where they help to understand jet-quenching phenomena. They also play a crucial role in the intermediate p_T region, being witness of a strong interplay between hard and soft processes.

The chemical composition analyses performed at SPS and RHIC, relying on thermal models based on chemical equilibrium conditions, successfully describe (strange) particle ratios in central collisions [1, 2]. This suggests that a chemically-equilibrated and strangeness-saturated medium has been reached, and that the creation of a QGP during the initial state could be the driving force towards this equilibrium. The predicted Wrobleski factor (λ_s), defined as the ratio between the newly created strange quark-antiquark pairs and the light ones ($2 < s\bar{s} > /(< u\bar{u} > + < d\bar{d} >)$), is also in good agreement with those data [3]. According to the predictions of the equilibrium statistical models, λ_s should be almost constant between RHIC and LHC, because of the very small variations expected for the temperature and the chemical potential at chemical freeze-out. However, according to non-equilibrium scenarios describing the sudden hadronisation of a QGP and implying an over-saturation of strangeness, one could observe a substantial increase of λ_s [4]. Therefore, it will be very interesting to estimate this quantity at LHC.

Strange quark production is predicted to be much larger in a QGP than in a hadronic system because of both gluon fusion mechanisms such as $gg \rightarrow s\bar{s}$ and partial chiral sym-

[*]IPHC-DRS, Strasbourg, France
[†]CERN, Geneva, Switzerland

metry restauration implying a lower effective mass for strange quarks [5]. This strangeness enhancement in A-A collisions, relative to hadronic reference systems such as p-p or p-Be, has indeed been observed both at SPS and at RHIC [6, 7]. Yet, this can be qualitatively described by statistical models in terms of canonical suppression, since the correlation volume, in which quantum numbers have to be conserved, is much smaller in the reference collisions, which implies a lower statistical strangeness production [8]. The predominance of hard parton scatterings at LHC energies might significantly affect the interpretation we have of this correlation volume, both in pp and Pb–Pb collisions. As already observed at RHIC, it may no longer be related only to the number of participant nucleons ($< N_{part} >$), but also to the amount of binary collisions ($< N_{bin} >$) [7]. In other terms, what will be the respective contributions of the source reflecting the equilibrated Grand Canonical Ensemble, and of the one relative to hard processes at LHC?

Concerning the expansion dynamics of the system, several results based on strange particles measured at RHIC have led to the indication that a deconfined medium has been created [2]. Indeed, it has been shown that all hadrons are exposed to a comparable elliptic flow (v_2) magnitude, even those expected to have low hadronic cross sections (like the Ξ or the Ω) [9], which seems to indicate that their flow originates from a partonic medium. The occurence of partonic degrees of freedom could be confirmed by the constituent quark scaling of v_2 observed at intermediate p_T, although this convenient explanation is not unique. It is clear that the differences observed between mesons and baryons ($\mathrm{K^0_S}$ and Λ in particular) concerning v_2 or nuclear modification factors at intermediate p_T, together with the unexpected high baryon/meson ratio, seem to reveal a strong interplay between hard and soft processes. This can be reasonably well reproduced by several approaches, one of them assuming a competition between two hadronisation mechanisms: parton recombination at low p_T and parton fragmentation at high p_T. Alternatively, combining a hydrodynamical behaviour with jet-quenching cannot be ruled out [10]. At LHC, where this hard-soft interplay is expected to increase and move towards higher p_T, the reconstruction of strange hadrons will again shed light on flavour and mesonic/baryonic dependence of in-medium effects. These studies will need, like at RHIC [11], detailed measurements in pp collisions, in order to first understand the elementary hadron production mechanisms involved.

The strange particles, such as $\mathrm{K^0_S}$, Λ, Ξ and Ω, will be identified in ALICE via topological methods based on their charged decay modes. Thus, their identification can be made from low to high transverse momenta without limitation, other than statistics. They will therefore allow numerous physical analyses concerning both soft and hard processes, in momentum ranges where traditional hadron identification (specific ionisation in TPC and ITS or time of flight measurements) fails or is more difficult to achieve.

In the first section of this note, we estimate the capability of the ALICE experiment to reconstruct $\mathrm{K^0_S}$ and hyperons, and we show that the studies related to the physics topics stated above are achievable after the first year of Pb–Pb data taking at LHC.

In the second section, our interest for a more exotic aspect of strangeness is presented. The proposal that strange dibaryons might exist as metastable states or resonances has stimulated a substantial activity on both the theoretical and experimental sides for many years. One may wonder about the ALICE capabilities to pursue this research in the future. We have addressed this question by evaluating the sensitivity of the ALICE detector to the discovery of such exotic strange clusters, concentrating on three hypothetical

strange dibaryons and applying the same reconstruction techniques as the ones used for hyperons.

1 Topological identification of K^0_S and hyperons

In this section, we show that the statistics of the first run of data taking in Pb–Pb (estimated to be 10^7 central events for a period of $\sim 10^6$ s at $\sqrt{s_{NN}} = 5.5$ TeV) should allow to determine the main characteristics of hyperon production with good precision, even for rare probes such as the Ω. The expected reconstructed yields as well as the range of transverse momentum (p_T) spectra are presented for different hypotheses. We also aim to evaluate the main analyses which will rely on this technique and give some prospects for others which should be available in a short term range. For instance, due to the large transverse momentum range of identification, anti-baryon/baryon, mixed and binary collision scaled centrality (R_{CP}) ratios should be statistically significant up to rather large transverse momenta (~ 10 GeV/c).

Firstly, we describe the simulated events we use and the selection strategies based on a compromise between efficiency and signal over background ratio (S/B). Then we present our best estimates of the expected efficiencies and reconstruction rates for neutral single strange particles (K^0_S, Λ) and charged multi-strange ones (Ξ, Ω) respectively. Finally we discuss the assumptions we used for these studies and the analyses which will be performed.

1.1 Simulation and selection strategies

A sample of 300 HIJING [12, 13, 14, 15, 16] events with a charged particle density per unit of pseudo-rapidity $\mathrm{d}N_{ch}/\mathrm{d}y = 4000$ (i.e. approximately the $0-10\%$ most central collisions) is considered for this study. In order to estimate detection efficiencies for strange particles, it is needed to generate realistic global production yields for these particles. Unlike the K^0_S, whose mean production rate in HIJING is about 260 per event, the ones of hyperons are low as compared to measurements taken at RHIC energies [17, 18, 19]: therefore, additional hyperons have been embedded in those events. The resulting multiplicities correspond to predictions for LHC [20] and from extrapolations of RHIC and TEVATRON data [21]. The momentum distributions are chosen according to m_T-scaling from pions [22] with characteristics shown in Table 1.

Particle	Λ , $\overline{\Lambda}$	Ξ^- , $\overline{\Xi}^+$	Ω^- , $\overline{\Omega}^+$
Embedded Particles	100	15	3
T (MeV)	650	700	800

Table 1: Number of hyperons embedded at $|\eta| < 0.89$ in central HIJING events and related inverse slope parameter (exponential distribution).

Definitions of the acceptance, efficiency and reconstruction rate of the hyperon reconstruction are explained below. The general notion of the acceptance corresponds to the probability for a given produced particle to be findable, or reconstructible. The acceptance depends on both the geometry and the physical properties of the detector.

We therefore have to define some criteria for a track to be labelled as 'findable', and those criteria must fit with the tracker requirements and abilities. Thus we call findable

a track that i) does not decay before the outer radius of the TPC; ii) that creates at least 70 clusters in the TPC; iii) whose pseudo-rapidity belongs to $[-1.05, +1.05]$. If one wants to reconstruct tracks using the ITS too, one can consider an additional condition on the number of clusters created by the track in the ITS layers.

We may extend the definition of a findable single track to that of a findable secondary vertex. Hence, we call findable a particle which decays inside a 'fiducial' zone, and whose daughter tracks are all findable for the weak decay channel we investigate. The decay channels considered in this section are: $\mathrm{K}^0_\mathrm{S} \to \pi^+\pi^-$ and $\Lambda \to \mathrm{p}\,\pi^-$ (so-called 'V^0' decays), and $\Xi^- \to \Lambda\,\pi^-$ and $\Omega^- \to \Lambda\,K^-$ ('cascade' decays).

The definition of acceptance (ACC) for a given particle X is the following:

$$ACC_X = \frac{\text{number of findable } X}{\text{number of generated } X}$$

As a consequence, the acceptance for a given particle is limited by its decay branching ratio, namely 68.9%, 63.9%, $99.9\% \times 63.9\%$ and $67.8\% \times 63.9\%$ for $\mathrm{K}^0_\mathrm{S}, \Lambda$, Ξ^- and Ω^- respectively. Similarly, we define the reconstruction efficiency (EFF) for a given particle X as:

$$EFF_X = \frac{\text{number of reconstructed findable } X}{\text{number of findable } X}$$

This efficiency describes the tracker and secondary vertex finder ability to reconstruct a findable particle for a given set of reconstruction cuts. We are able to differentiate a fake (wrong association of tracks) from a findable reconstructed secondary vertex thanks to a Monte-Carlo tagging procedure.

Finally the reconstruction rate (ϵ_X) of a given particle X is defined as the product of ACC_X and EFF_X (i.e. the probability to reconstruct a generated particle):

$$\epsilon_X = ACC_X \times EFF_X = \frac{\text{number of reconstructed findable } X}{\text{number of generated } X}$$

Using a magnetic field of 0.5 T for momentum determination, several reconstruction strategies have been evaluated differing on the size of the fiducial region and the track selection.

The first one consists of limiting the secondary vertex reconstruction to a very narrow fiducial zone inside the beam pipe, i.e. a cylindrical zone whose inner and outer radii are respectively 0.9 and 2.9 cm in the transverse plane. This way, the strange particle daughter tracks may create clusters in each of the 6 layers of the ITS; one may thus benefit fully of the ITS resolution, and reduce the background coming from primary particle combinations and secondary particles produced in the beam pipe material.

With this first approach it is possible to obtain clean signals (with a S/B of the order of 10), especially for the K^0_S and for the Λ, the counterpart being a small reconstruction rate ($< 1\%$) for all strange particles. It is especially the case at high transverse momentum (p_T) since the decay is likely to happen outside this zone. This results from both the acceptance ($\sim 4\%$) in a small fiducial zone and from the selection of high quality tracks which must contain one cluster in every ITS layer. This is illustrated in Fig. 1 showing the extent of the reconstruction region together with the radius of the ITS layers and the $c\tau$ of the hyperons (which corresponds to the mean decay length when $\beta\gamma = 1$).

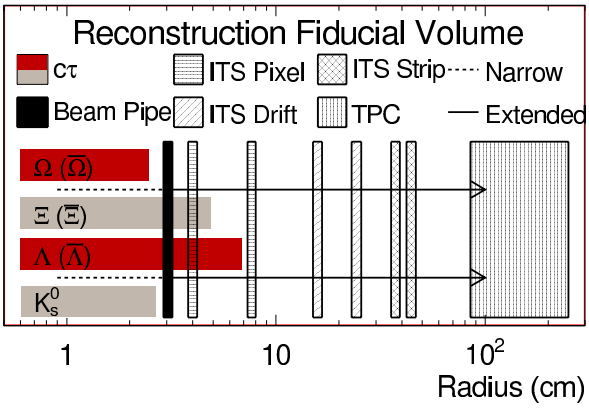

Figure 1: Fiducial zone for strange and multi-strange particles together with their $c\tau$. The extended radius reaches $R_{max} = 100$ cm.

In order to increase the reconstruction rates, especially at high p_T, a second strategy has been investigated. It consists of performing the secondary vertex reconstruction with all the tracks available in the TPC and no further selection based on the number of ITS clusters. However the information given by the ITS for determining vertex characteristics is used when available. In such a case, the reconstruction zone radius can be larger than that of the last ITS strip layer and extended up to the inner TPC radius. As this limit may even be chosen to be inside the TPC, the extended radius has been set to $R_{max} = 100$ cm for this study.

1.2 Single strange particle identification in Pb–Pb collisions: Λ and K^0_S

For Λ particles, the extended area of the reconstruction zone results in a rise of the acceptance to an average value of 25% (when integrated over the whole p_T range). The gain is especially significant at high p_T where a 'plateau' at $\sim 40-50\%$ is reached with a slight decrease after 6 GeV/c as illustrated in Fig. 2.

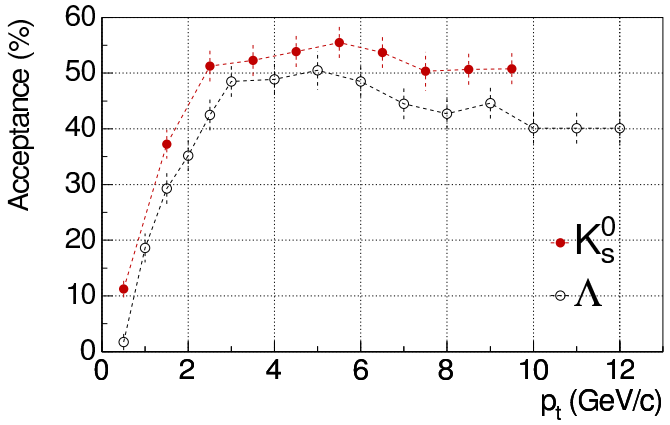

Figure 2: Acceptance of K^0_S and Λ particles as a function of p_T for a V^0 vertex reconstruction zone extending up to a radius $R_{max} = 100$ cm.

With this strategy, the secondary vertex parameters are determined with a reduced accuracy, on the average, compared to those whose daughter tracks contain 6 ITS clusters. Therefore, the geometrical selections on the V^0 parameters (e.g. on the distance of closest

approach (DCA) between the positive and negative daughter tracks, see Fig. 3) must be loosened, but the consequence is a higher level of background. However, while maintaining a high efficiency, the S/B can still be improved by tightening the cuts on the track parameters (e.g. setting the minimum impact parameters of the daughters to higher values) as well as applying stringent kinematic selections.

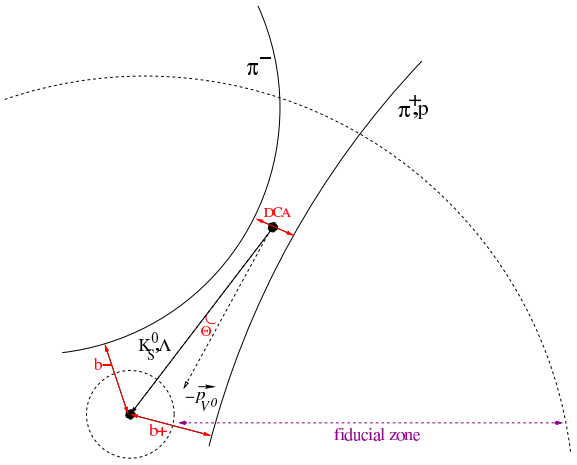

Figure 3: Geometrical selections used for V^0 reconstruction.

Fig. 4 shows the distributions of geometrical quantities, corresponding respectively to $cos\Theta$, DCA, b_-, and b_+ (see Fig. 3), for the Λ signal and the Λ combinatorial background, together with a set of selections used as reference for reconstruction. This set is optimised to obtain the best compromise between signal efficiency and a low level of background. The selections for Λ particles are described below:

- cosine of Λ pointing angle: $\cos\Theta > 0.999$;
- distance of closest approach between Λ daughters: DCA< 0.5 cm;
- impact parameter for the meson daughter of Λ: $b_- > 0.15$ cm;
- impact parameter for the baryon daughter of Λ: $b_+ > 0.1$ cm.

Additional kinematic conditions are required to further reduce the background. Namely a minimum transverse momentum value of 180 MeV/c for the meson (i.e. pion) and 600 MeV/c for the baryon (i.e. proton). The corresponding distributions are shown in Fig. 5.

Particle	Generated per event in $\|\eta\| < 0.89$	ACC (%)	EFF (%)	Reconstructed per event	S/B
K^0_S	264	15.0 ± 0.5	58.1 ± 0.1	23 ± 0.3	1.5
Λ^0	100	25.5 ± 0.3	43.0 ± 0.6	11 ± 0.2	1.5

Table 2: Estimated production yields, mean acceptances, efficiencies, reconstruction yields and signal to background ratios for a reconstruction region restricted to $0.9 < R < 100$ cm and for reference selections. Errors are statistical.

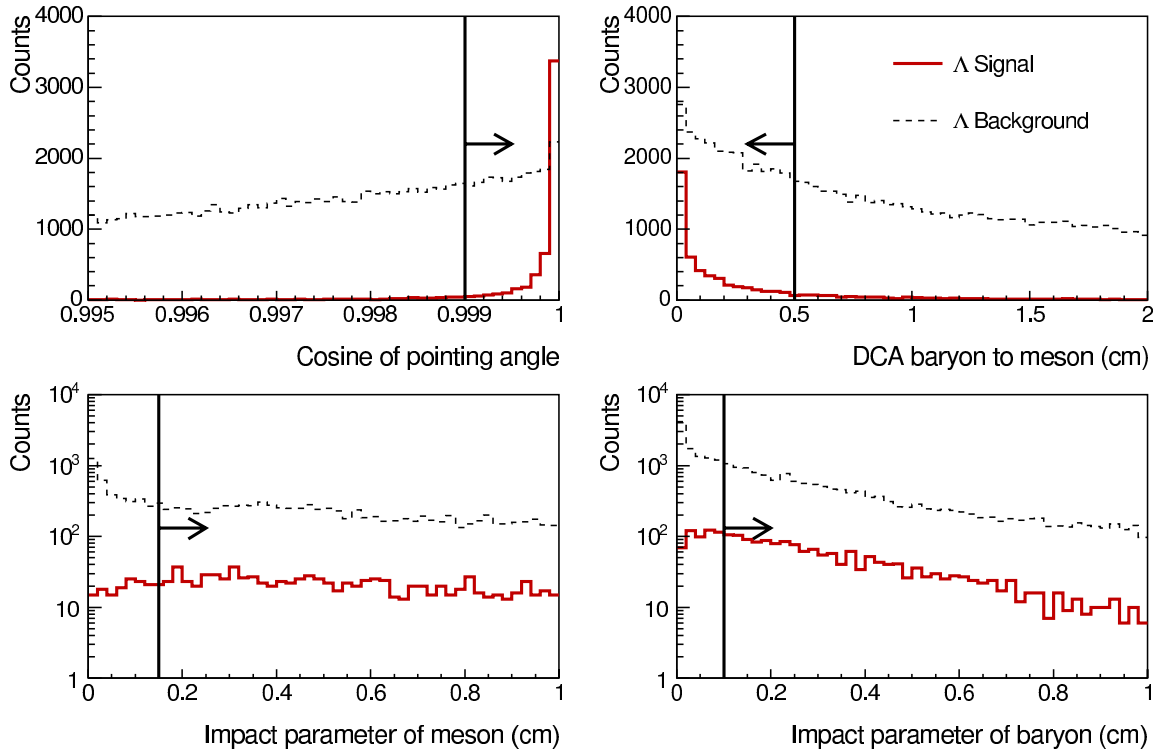

Figure 4: Distribution of the geometrical quantities for Λ signal (plain) and background (dashed) for: i) the cosine of the pointing angle (upper left panel); ii) the DCA between positive and negative tracks (upper right panel); iii) impact parameters of the meson and baryon daughters of the Λ (respectively left and right lower panels). The areas kept by the geometrical selections are indicated by the arrows.

Using this set of cuts, an average efficiency of 43% and a reconstruction yield of ~ 11 per event were obtained for the Λ. These estimates rely on the production yields and the related transverse momentum distributions as given in Table 1. The relevant reconstruction information for Λ and K^0_S is gathered in Table 2. The left panel of Fig. 6 shows the Λ invariant mass distribution obtained under these conditions.

> *Note*: in order to have an upper limit for the multiplicity dependence of these results and given the uncertainty range on the maximum track density prediction at LHC, Λ reconstruction has also been studied for $dN_{ch}/dy = 6000$. Using the reference selections quoted above, the corresponding average efficiency, reconstruction rate and S/B are found to be 38%, 9.6% and 0.3 respectively.

At $dN_{ch}/dy = 4000$, the p_T distribution is shown in the right panel of Fig. 6 with a S/B larger than unity over the whole p_T range except below 1 GeV/c.

For the K^0_S reconstruction, the global acceptance value is $\sim 15\%$. We obtain an average efficiency of 58%, which provides a reconstruction yield of 23 K^0_S per event when using input from Table 1 and the following selections:

- cosine of K^0_S pointing angle: $\cos\Theta > 0.998$;
- distance of closest approach between K^0_S daughters: DCA < 0.5 cm;

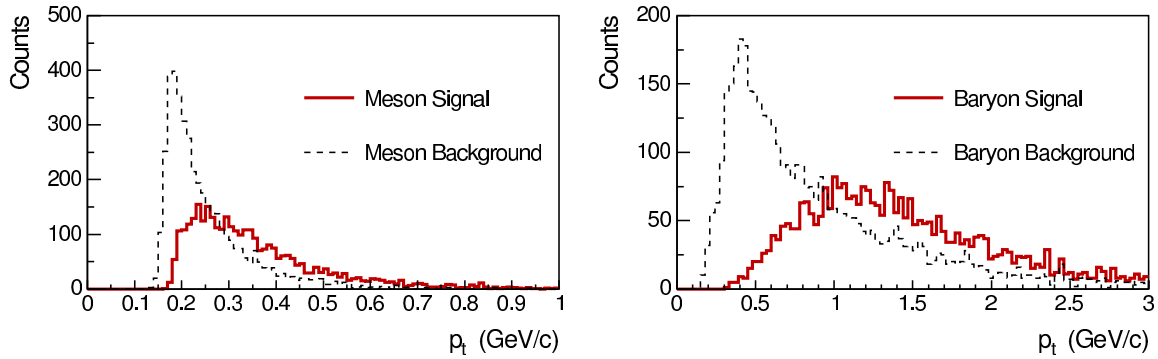

Figure 5: Transverse momentum distributions of the Λ daughters' signal (plain) and combinatorial background (dashed).

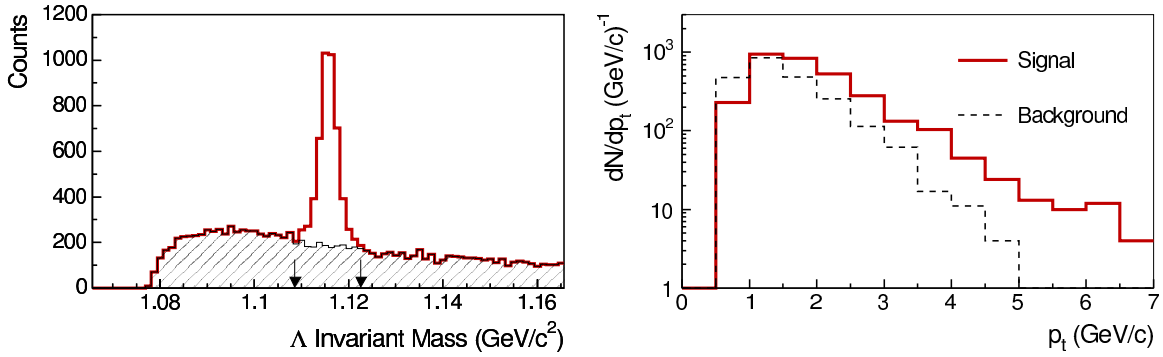

Figure 6: Λ invariant mass spectrum obtained after the reference set of selections (see text) have been applied on 300 reconstructed HIJING events (left panel). Signal (plain) and background (dashed) as a function of p_T for reconstructed Λ for the same 300 HIJING events.

- impact parameter for the negative daughter of K^0_S: $b_- > 0.07$ cm;
- impact parameter for the positive daughter of K^0_S: $b_+ > 0.07$ cm.

For the Λ reconstruction, if we release the conditions on the daughter impact parameters ('loose' selections) in the following way: $b_- > 0.1$ cm, $b_+ > 0.05$ cm and increase the maximum DCA to 1 cm, the efficiency goes up to 55.5% (more than 14 reconstructed Λ per event) but the global background level becomes significantly higher (S/B= 0.9). This is shown in the left panel of Fig. 7. Nevertheless, as presented in this figure (right), the background dominates only at low p_T. For $p_T > 2$ GeV/c, the background clearly drops below the signal amplitude. Therefore, this set of selections can be used to increase the efficiency for Λ particles at intermediate and high p_T.

For any set of cuts and $p_T > 5$ GeV/c, the efficiency decreases slowly with increasing p_T, due to two main reasons. The first one corresponds to the fact that the vertices are determined with less and less precision as the V^0 decay position moves away from the main vertex, since the daughter tracks create fewer clusters in the detectors. The

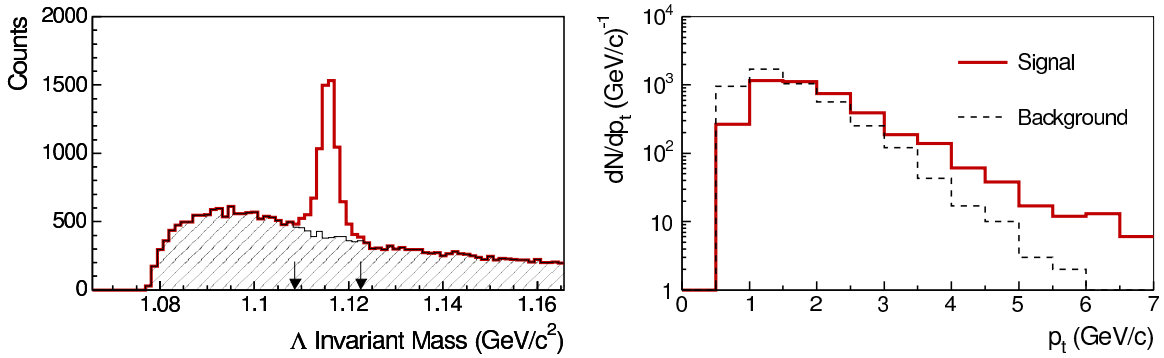

Figure 7: Left panel shows the Λ invariant mass spectrum, corresponding to the 'loose' set of selections and obtained for the reconstruction of 300 HIJING events. The right panel corresponds to the Λ signal (plain) and background (dashed) as a function of p_T, obtained for the reconstruction in 300 HIJING events with the same selections.

second reason is geometrical: the high p_T of the V^0 causes the impact parameters to reduce, and thus not to satisfy the minimum criteria on b^- and b^+. To prevent such a decrease in efficiency, the cuts must be loosened. We therefore loosen the requirements on the minimum impact parameter with increasing p_T. This is illustrated in Fig. 8 which compares the b^- distributions for two different momentum ranges of the Λ: $1 < p_T$ (GeV/c) < 2 and $10 < p_T$ (GeV/c) < 12.

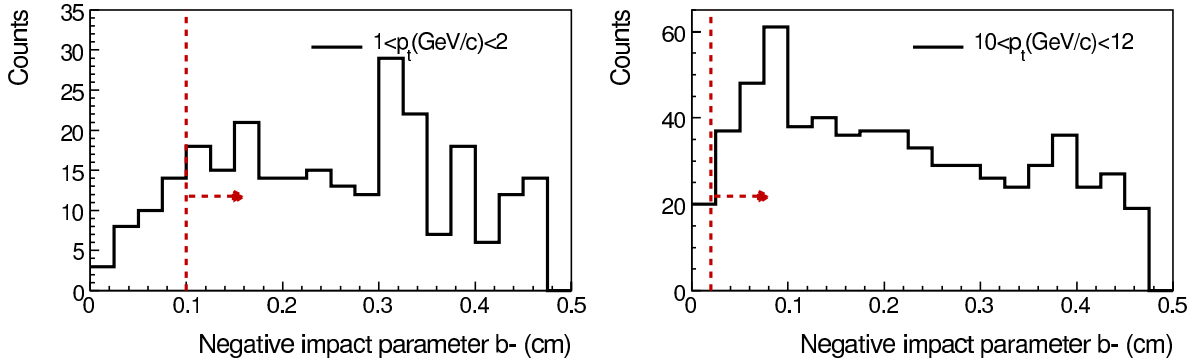

Figure 8: Comparison between the negative impact parameter (b_-) distributions for two different momentum ranges: $1 < p_T$ (GeV/c) < 2 (left panel) and $10 < p_T$ (GeV/c) < 12 (right panel) with the corresponding selections (arrows) for Λ reconstruction.

In order to take advantage of these trends, a set of p_T-dependent selections has been built, so as to improve the efficiency at intermediate and high p_T, while keeping the background low (S/B > 1) over the whole p_T range (except for $p_T < 1$ GeV/c). The p_T-dependent selections are defined for four p_T ranges as shown in Table 3, where the selections on the DCA and the impact parameters are loosened with increasing p_T .

p_T range (GeV/c)	$\cos\Theta$	DCA (cm)	b_-(cm)	b_+(cm)
$[0-2.5]$	> 0.999	< 0.5	> 0.10	> 0.05
$[2.5-4.5]$	> 0.999	< 1.0	> 0.10	> 0.05
$[4.5-8]$	> 0.999	< 1.0	> 0.06	> 0.03
$[8-12]$	> 0.999	< 1.0	> 0.02	> 0.01

Table 3: Transverse momentum dependent selections for Λ reconstruction (see Fig. 9).

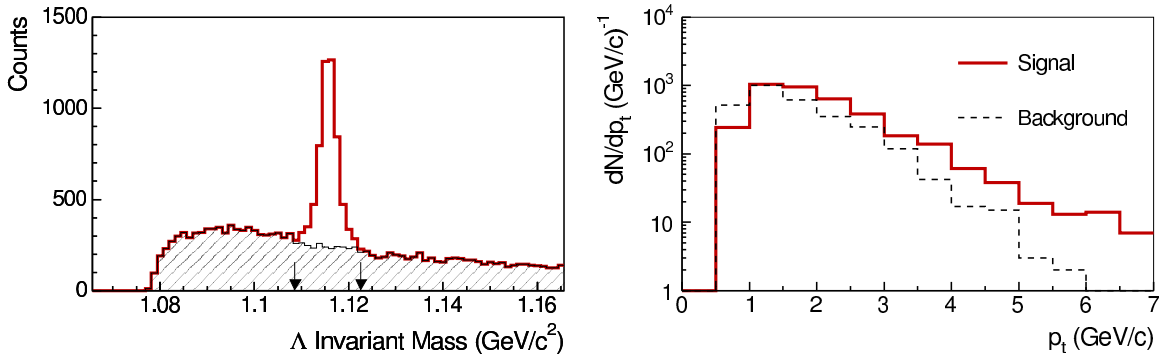

Figure 9: Λ invariant mass spectrum obtained with the p_T-dependent selection set (left panel). Corresponding signal (plain) and background (dashed) distributions as a function of p_T (right panel).

When compared to reference selections (see Table 2), the efficiency integrated over the whole p_T range shows a substantial increase ($50.0 \pm 0.6\%$ instead of 43%), whereas the global S/B is only slightly reduced (from 1.5 to 1.2). The corresponding yield of reconstructed Λ reaches 13 (± 0.2) per event to be compared to 11. These results are illustrated in Fig. 9.

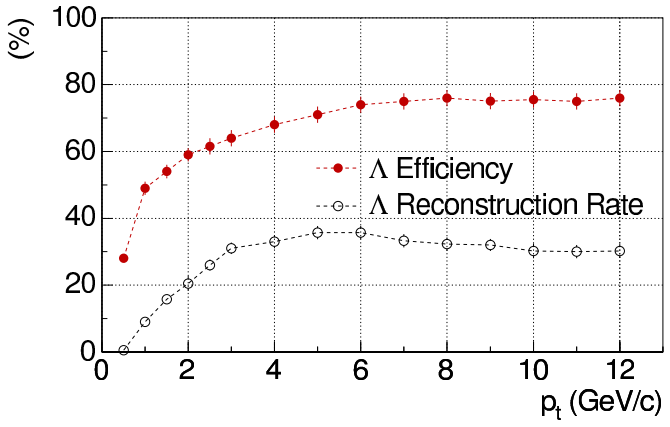

Figure 10: Efficiency and reconstruction rate as a function of transverse momentum for Λ particles, obtained with p_T-dependent selections.

The reconstruction efficiency profile resulting from the p_T-dependent selections is shown in Fig. 10 together with its product with the acceptance (see Fig. 2), which gives the reconstruction rate for Λ particles. The Λ p_T spectra are shown in the left panel

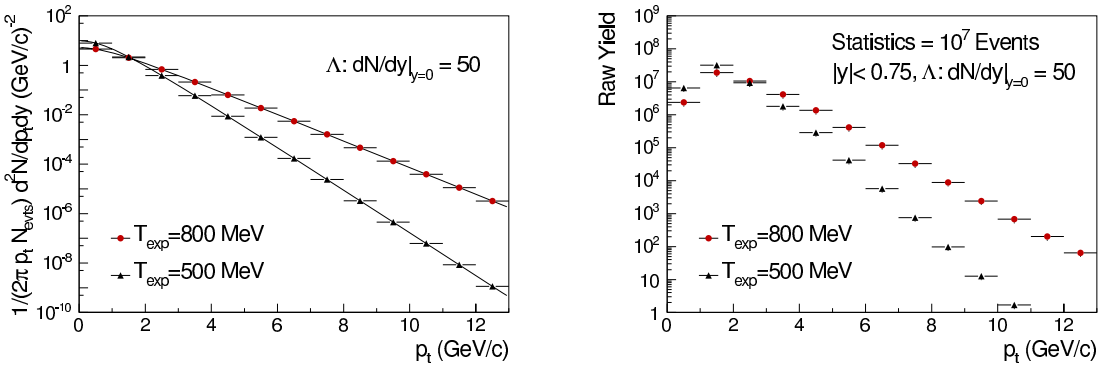

Figure 11: Left panel: Generated p_T spectra of Λ particles for two hypotheses of inverse slope parameter (exponential functional form) and an estimated production yield at mid-rapidity of 50. Errors are from the simulation statistics. Right panel: Reconstructed Λ (raw spectra) distributions corresponding to the convolution of inclusive p_T spectra with the reconstruction rate and for a total statistics of 10^7 central Pb–Pb events.

of Fig. 11 for two hypotheses. They define a likely interval for the expected spectra at LHC for central Pb–Pb collisions, assuming a production yield of 50 Λ per event. The upper and lower estimate depends on the assumed transverse radial flow for the Λ particles: the generated exponential p_T-spectra correspond respectively to inverse slopes of 800 MeV and 500 MeV. The convolutions of these spectra with the Λ reconstruction rate are shown in the right panel and provide an estimate of the inclusive reconstructed spectrum at mid-rapidity. We can conclude that with a total of 10^7 central events, Λ particles should be reconstructed at least up to $p_T = 10$ GeV/c.

1.3 Multi-strange particle identification in Pb–Pb collisions: Ξ and Ω

Assuming the inverse slope parameters presented in Table 1, the integrated acceptances for the reconstruction of Ξ and Ω are $9\pm0.4\%$ and $5.8\pm0.2\%$ respectively. The acceptance evolution as a function of p_T at mid-rapidity is shown in Fig. 12. The slight decrease for high p_T particles is due to the finite fiducial zone, stopping in the TPC.

For cascade (charged Ξ or Ω) identification in the Pb–Pb environment, we first select the likely secondary Λ from the V^0 sample (see Fig. 13). The selection of the Λ daughters corresponds to minimum values of impact parameter which are close to the ones used for primary Λ. However, the condition on the DCA of the Λ daughter tracks is strengthened in order to limit the combinatorial background. Further conditions are required for the Λ candidate, such as a minimum impact parameter to the primary vertex and an invariant mass range selection. Since these Λ are secondary, the V^0 pointing angle to the primary vertex selection must be kept loose. The bachelor candidate must have a small DCA to the Λ trajectory while its impact parameter has a minimum value for selecting a secondary particle. Finally, the reconstructed cascade must point back to the primary vertex. Therefore a minimum value for the cosine of its pointing angle is used. The selections and values used for Ξ and Ω studies are shown in Table 4.

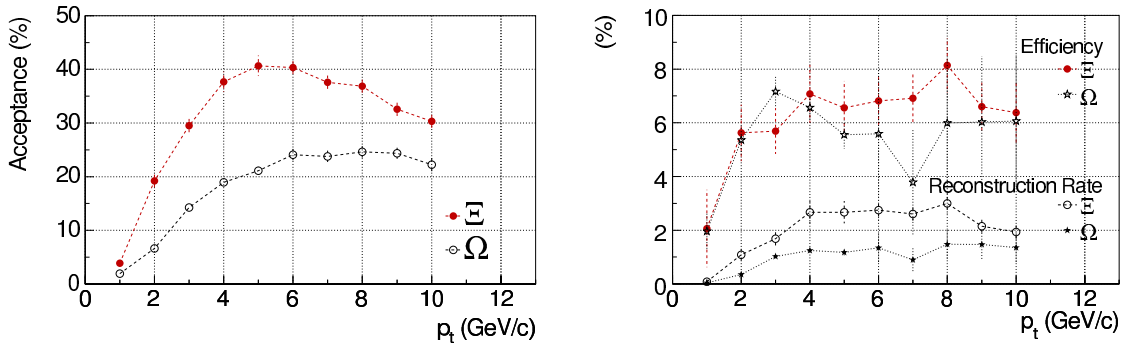

Figure 12: Left panel: Acceptance for Ξ and Ω reconstruction as a function of p_T. Right panel: Efficiency and reconstruction rate as a function of transverse momentum for Ξ and Ω particles obtained with quoted selections for identification (see text).

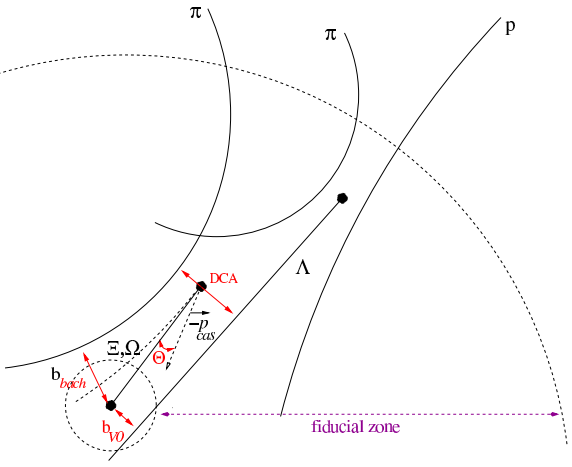

Figure 13: Geometrical selections used for cascade reconstruction

Selection		Ξ	Ω
impact parameter for the meson daughter of Λ:	b_-	> 0.2 cm	> 0.25 cm
impact parameter for the baryon daughter of Λ:	b_+	> 0.06 cm	> 0.1 cm
DCA between Λ daughters:	$\mathrm{DCA}_{(-,+)}$	< 0.1 cm	< 0.08 cm
cosine of Λ pointing angle:	$\cos\Theta_{V0}$	> 0.995	> 0.996
invariant mass window around the Λ mass:	$\lvert m_\Lambda - 1115.68\rvert$	< 5 MeV/c^2	< 3 MeV/c^2
impact parameter for the Λ:	b_Λ	> 0.1 cm	> 0.2 cm
impact parameter for the bachelor:	b_b	> 0.12 cm	> 0.1 cm
DCA between the bachelor and the Λ candidate:	$\mathrm{DCA}_{(\Lambda,b)}$	< 0.1 cm	< 0.08 cm
cosine of cascade pointing angle:	$\cos\Theta_\Xi$	> 0.9995	> 0.9996

Table 4: Geometrical selections used for Ξ and Ω reconstruction in Pb–Pb events.

Due to the limitated statistics of the simulated data, no further optimisation, as a function of p_T, has been considered so far. Also PID will significantly enhance the S/B and will be used for distinguishing Ω signal from Ξ via their decay daughter (kaon instead of pion). The Ξ and Ω invariant mass spectra obtained from this set of selections are

shown on Fig. 14. The estimated reconstruction efficiency for the Ξ (Ω) is close to $5 \pm 1\%$ ($6 \pm 0.8\%$) on average which gives a Ξ (Ω) reconstruction yield of 0.075 ± 0.02 (0.01 ± 0.001) per event.

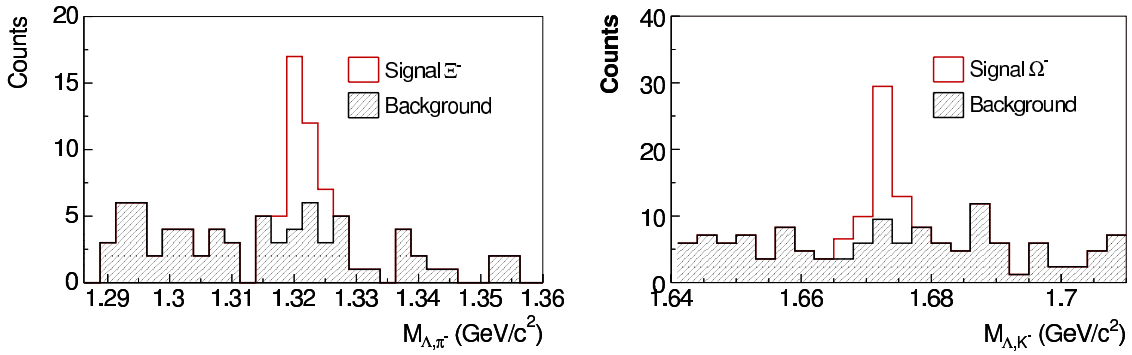

Figure 14: Left panel: Ξ invariant mass spectrum obtained via the reconstruction of 300 HIJING events. Right panel: For the Ω particle, a dedicated study was performed due to the low expected production yield (see Table 1); the shown invariant mass spectrum is an estimation of what should be obtained with 5000 HIJING events.

The reconstructed cascade p_T spectra are shown on Fig. 15 for two inverse slope hypotheses: T= 550 and 850 MeV.

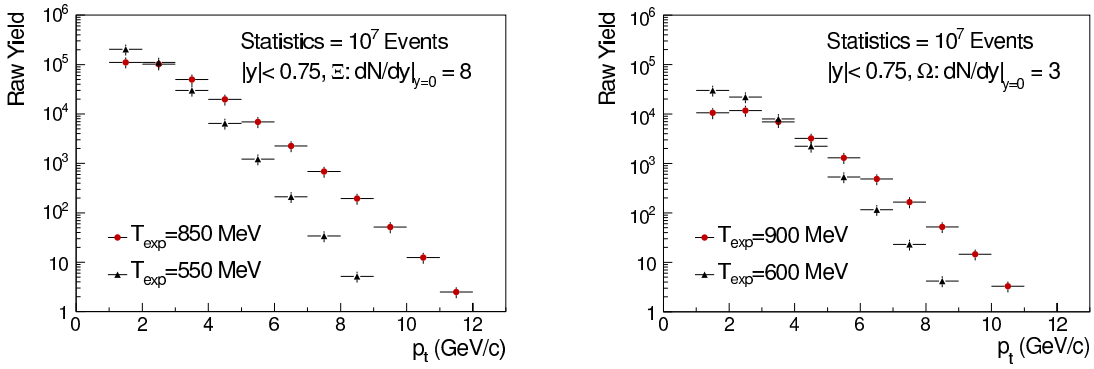

Figure 15: Estimation of reconstructed cascade (raw spectra) p_T distributions corresponding to the convolution of inclusive p_T spectra with the reconstruction rate for a total statistics of 10^7 central Pb–Pb events for Ξ (left panel) and Ω (right panel). Errors are statistical.

1.4 Discussion on single and multi-strange particles

From the performed simulations and under the assumptions made, transverse mass spectra for weak decaying single and multi strange particles should be available up to $\sim 8-10$ GeV/c after the first run of Pb–Pb data taking at LHC. This will not only provide the measurement of the production yields with a good accuracy (which is necessary for

the feed down correction of lower mass particles), but it will also make it possible to investigate the shape of the spectra in detail.

Nevertheless, the results presented here may be affected by systematic errors, sensitive to the chosen simulation parameters such as event multiplicities, strange particle p_T/y distributions and production yields, or magnetic field intensity.

For this purpose, we have studied the influence of the hyperon p_t distribution inverse slopes. Indeed, as the shapes of the real spectra might differ strongly from the simplified parameterisations which were assumed, we have shown the particle spectra obtained for two inverse slope parameters corresponding to expected low and a high estimates (Fig. 11 and 15). Actually, a substantial hard scattering contribution (depending on the coupling with a suppression) would lead to higher production yields than assumed at intermediate and high p_T. On the other hand, one may observe exactly the opposite trend if hyperons decouple from the medium at early times, and thus do not undergo the thrust coming from its inner pressure gradients (radial flow).

In any case, we expect the statistics and the range of identification to be sufficiently large to study possible coalescence mechanisms (with baryon/meson spectra), transverse radial flow effect and nuclear modification factors, in order to investigate the different hadronisation scenarios [23].

2 Topological identification of strange dibaryons

2.1 The H-dibaryon

Early predictions suggest that a six quark bag bound state ($uuddss$), may exist, because the colour magnetic forces are attractive and thus allow its ground state to be below the strong decay threshold ($M_{\Lambda\Lambda}$ = 2231 MeV/c^2) [24, 25]. This configuration with hypercharge Y = 0 (charge = 0, spin = 0, isospin = 0 and S = −2) is called the H-dibaryon (H^0). According to these predictions, it may not be stable against weak hadronic decay and its most probable mass range is [2055-2231] MeV/c^2. In this region, the H^0 can decay to Λn or ΣN (N=nucleon) (if $m_{H^0} > 2134$ MeV/c^2) and $\Lambda N\pi$ (if $m_{H^0} > 2195$ MeV/c^2). The lifetimes associated with these various decay modes are predicted to be in the interval [10^{-10}–10^{-8}] s.

The H^0 could also be a resonance (if $m_{H^0} > 2231$ MeV/c^2) decaying to $\Lambda\Lambda$, ΞN or $\Sigma\Sigma$. If this resonance lies only a few MeV/c^2 above the strong decay threshold, it may be experimentally observed by analysing the baryon-baryon continuum invariant mass spectrum [26].

2.2 Strange hadronic dibaryons

The hadronic counterpart to the H^0 is the so-called dilambda $(\Lambda\Lambda)_b$, a bound state of two Λ, with the same quantum numbers and the same decay channels as the H^0. Actually, many other dibaryon bound states might exist according to predictions using weak SU(3) symmetric contact interactions; these provide estimates of their corresponding weak hadronic decays as well as their lifetimes [27]. Production estimates for RHIC were also made by combining transport simulations with wave function coalescence using RQMD [28, 29]. Examples of such predicted dibaryons are the following: $(\Sigma^+\mathrm{p})_b \rightarrow \mathrm{pp}$, $(\Xi^0\mathrm{p})_b \rightarrow \Lambda\mathrm{p}$, $(\Xi^0\Lambda)_b \rightarrow \Xi^-\mathrm{p}$ or $(\Xi^0\Xi^-)_b \rightarrow \Xi^-\Lambda$.

With binding energies of a few MeV, their predicted decay lengths ($c\tau$) are between 1 and 5 cm. The predicted production yields, in central Au+Au collisions at $\sqrt{s_{NN}} = 200\ GeV$, vary from $5 \cdot 10^{-3}$ dilambda per unit of rapidity, which is rather high, down to smaller values if multi-strange hyperon combinations are considered: 10^{-4}/event for $(\Xi^0\Xi^-)_b$.

Experimentally, these decay topologies can be identified with an appropriate tracking device. For instance in the case of $(\Xi^0\mathrm{p})_b$ bound state, one has to find secondary Λ vertices associated with a proton track (bachelor). Such a procedure is comparable to the one applied to Ω or Ξ decay reconstruction (see Section 1), the K^- or the π^- bachelors being replaced by a proton.

2.3 The search for strange dibaryons in the central barrel of ALICE

In the following, we study the capability of the central barrel of ALICE to identify the H^0 particle or strange hadronic dibaryon. We first focus on weak decay modes via the topological method described in Section 1. Finally a strong decay resonance state is considered.

The identification of one of the H^0 possible weak decay modes, $H^0 \to \Sigma^- p \to n\pi^- p$, is very challenging because of the huge multiplicity of Pb–Pb collisions at LHC energies and the undetected neutron. The second weak decay mode, $H^0 \to \Lambda p\pi^- \to p\pi^- p\pi^-$, can however be observed with the ALICE detector if its two successive weak decays are reconstructed. The hadronic dibaryon $(\Xi^0 p)_b$ identification via a weak decay mode: $(\Xi^0 p)_b \to \Lambda p$ will be studied as well. Finally, we report the analysis corresponding to an H^0 strong decay mode, the $H^0 \to \Lambda\Lambda$.

2.4 The $H^0 \to \Lambda p\pi^-$ weak hadronic decay

For the H^0 properties, a lifetime of the same order of magnitude as for the Λ (i.e. $\tau \sim 2 \cdot 10^{-10}$ s) and a mass of 2210 MeV/c^2 were chosen. We note however that recent measurement of a double-Λ hypernucleus suggests a weak attractive $\Lambda\Lambda$ interaction and would mean slightly higher masses (just below $m_{\Lambda\Lambda}$) [30]. The rapidity distribution is constant and limited to the midrapidity region ($|y| < 1$). An exponential functional form was used for the transverse momentum distribution.

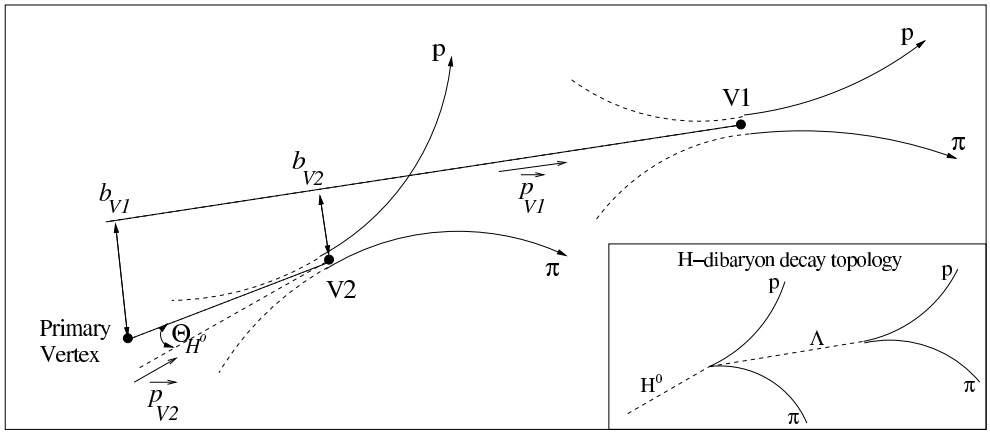

Figure 16: $H^0 \to \Lambda p\pi^-$ reconstruction procedure.

As a first step, we reconstruct all the secondary ($p\pi^-$) vertex (V^0) candidates. Then we find the V^0-V^0 associations that could correspond to an H^0 decay. The principle of the method is shown in Fig. 16. For each possible association between two ($p\pi^-$) vertices (V1,V2), starting here with V1, we calculate the V1 mother momentum ($\overrightarrow{p_{V1}}$) and its invariant mass. It is kept if this mass is close to the Λ mass (Δm_{V^0}). Then we require its momentum vector points back to the V2 vertex (selection on b_{V2}). A minimum value of the V1 impact parameter (b_{V1}) is also required to reduce the contamination from primary Λ candidates. Finally we calculate the V2 mother momentum ($\overrightarrow{p_{V2}}$), assuming that this vertex corresponds to a $p\Lambda\pi^-$ emission. If the candidate momentum vector points correctly back to the primary vertex (selection on the $\cos\Theta_{H^0}$), it is selected as an H^0 candidate and its invariant mass is computed. From this study, we obtain the reconstruction efficiency as well as the combinatorial background level.

A dedicated simulation including H^0 mixing with realistic HIJING events, detector digitisation and full event reconstruction (space point finding and tracking) was performed. This acceptance and efficiency study would require $\sim 10^5$ events because of the

expected low production yield of H^0 per event (less than one). Therefore we first generated events containing only H^0 (several tens of thousands per event). Out of these, only a few H^0 were findable, (a total of ~ 650), i.e. made of two findable V^0 (see Section 1). The acceptance (ACC) of the H^0 decay chain is defined as the ratio of the number of findable H^0 to the number of generated ones. This acceptance factor was found to be $0.48 \pm 0.02\%$.

Then the H^0 reconstruction efficiency (EFF), including the secondary track finding and V^0 reconstruction efficiencies, was estimated using 'signal enriched' events, i.e. HIJING events with a particle density of $\mathrm{d}N_{ch}/\mathrm{d}y = 4000$, mixed with only the findable H^0 selected in the previous step.

Table 5 presents the cuts corresponding to both V^0 (left side) and H^0 (right side) reconstruction procedures. Applied to the set of events stated above, these cuts allow one to identify 23 H^0.

cuts on V^0				cuts on H^0			
b_-^{min}	b_+^{min}	DCA^{max}	$\cos\Theta_\Lambda^{min}$	b_{V1}^{min}	b_{V2}^{max}	$\Delta m_{V^0}^{max}$	$\cos\Theta_{H^0}^{min}$
0.25 cm	0.02 cm	0.045 cm	0.955	0.04 cm	0.05 cm	$\pm 7 MeV/c^2$	0.9999

Table 5: Geometrical selections used for the identification of $H^0 \to \Lambda \mathrm{p}\pi^-$.

The quantity EFF, defined as the ratio of the number of found H^0 to the number of findable ones, is therefore $3.5 \pm 0.7\%$. The rate (ϵ) of reconstructed H^0 is then given by the acceptance factor multiplied by the reconstruction efficiency:

$$\epsilon = EFF \times ACC = (1.7 \pm 0.36) \cdot 10^{-2}\ \%$$

The extracted signal of 23 found H^0 would correspond to about $23/\epsilon = 135000$ events if we assume that the multiplicity of produced H^0 in the detector acceptance is one per event. The next step consists of evaluating the background level corresponding to this set of events. Here, we assume that wrong associations between a primary and a 'signal' track, coming either from a hyperon or from an H^0, constitute the dominant part of the background.

We generated $N = 15$ HIJING events and $M = 9000$ 'pure signal' events with the expected multiplicity of the 'signal' particles (see Table 1). Then we combine the tracks from each of the N HIJING events with each of the M signal events. After reconstructing $N \times M$ such mixed track sets, we obtain a background statistically equivalent to $N \times M$ 'signal+HIJING' events. The resulting background is shown in Fig 17, together with the corresponding H^0 signal. In the mass window around 2210 ± 7 MeV/c^2, shown in the invariant mass spectrum, the background level is less than 10 counts.

The last step is to extrapolate this background to the full expected statistics, $N_{\mathrm{event}} \sim 10^7$ central events and hence deduce the detection sensitivity. We find that the observation of an H^0 signal, above the background at a 3-σ confidence level, requires the reconstruction of $n_{\mathrm{H^0}} \simeq 80$ H^0s. Here σ represents the significance of the signal, i.e. the ratio $S/\sqrt{N}$, S and N being respectively the number of signal and background counts in the mass window $[2210 \pm 7]$ MeV/c^2.

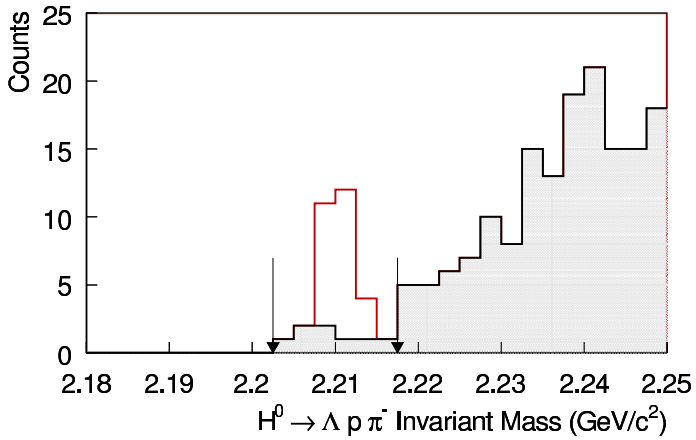

Figure 17: $\Lambda p\pi^-$ invariant mass spectrum for $H^0 \to \Lambda p\pi^-$ reconstruction in ALICE, for 135000 simulated Pb–Pb central events at 5.5 TeV ($dN_{ch}/dy = 4000$), assuming an average production yield of 1 H^0 per event in the $|y| < 1$ rapidity range.

The sensitivity (S_{H^0}) is defined as this number divided by the total number of analyzed events times ϵ:

$$S_{H^0} = n_{H^0}/(\epsilon \times N_{\text{event}})$$

The sensitivity obtained is about $5 \cdot 10^{-2}$ H^0/event over the two covered units of rapidity, hence $dN_{H^0}/dy = 2.5 \cdot 10^{-2}$ H^0 per event in this rapidity range.

2.5 The $(\Xi^0 p)_b \to \Lambda p$ weak hadronic decay

For this study, we have chosen a $(\Xi^0 p)_b$ lifetime of $\tau = 2.6 \cdot 10^{-10}$s and a mass of 2225 MeV/c^2. Such a mass corresponds to a binding energy of about 30 MeV.

The principle of the reconstruction algorithm for the $(\Xi^0 p)_b$ is the same as for the Ξ decay to $\Lambda\pi$ except the π is replaced by a proton. Then, applying the same procedure and definition as for H^0 reconstruction, we found the following results: $ACC = 0.57 \pm 0.03\%$ and $EFF = 9.64 \pm 1.62\%$, which leads to a rate of reconstructed $(\Xi^0 p)_b$ of $(5.5 \pm 0.96) \cdot 10^{-2}$ %.

The invariant mass distribution shown in Fig. 18 contains a signal of 32 found $(\Xi^0 p)_b$. It corresponds to $\sim$ 60000 events with a production yield of 1 $(\Xi^0 p)_b$ per event. The background under the peak is less than 20 counts. Extrapolated to 10^7 events, this result shows that the 3-σ evidence of such a dibaryon needs a minimum number of 180 reconstructed $(\Xi^0 p)_b$, which requires in turn a minimum number of $\sim 3.5 \cdot 10^{-2}$ $(\Xi^0 p)_b$ produced per event in the region $|y| < 1$. We conclude that the production yield should be at least $dN_{H^0}/dy = 1.7 \cdot 10^{-2}$ $(\Xi^0 p)_b$ for this particle to be observed.

2.6 The $H^0 \to \Lambda\Lambda$ strong decay resonance

In this section we describe the search for an H-dibaryon strong decay resonance in Pb–Pb collisions. The mode under consideration is $H^0 \to \Lambda\Lambda$. To predict the ability of the ALICE detector to identify such objects, we start by creating 300 HIJING events with a

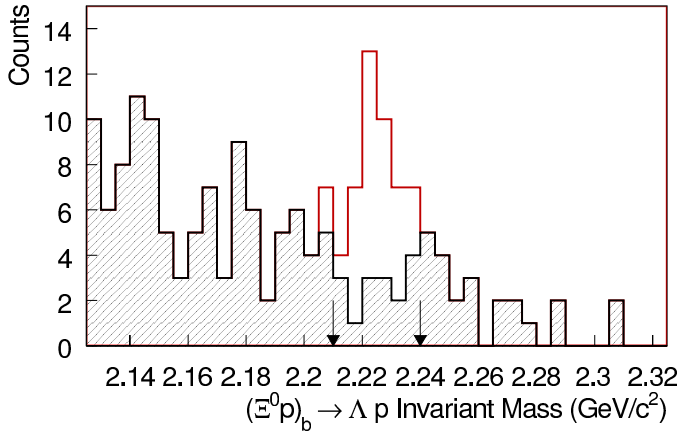

Figure 18: Λp invariant mass spectrum for $(\Xi^0\mathrm{p})_b \rightarrow \Lambda\mathrm{p}$ reconstruction in ALICE, for 58000 Pb–Pb central events at 5.5 TeV ($\mathrm{d}N_{ch}/\mathrm{d}y = 4000$), assuming an average production yield of 1 $(\Xi^0\mathrm{p})_b$ per event in the range $|y| < 1$.

realistic background ($\mathrm{d}N_{ch}/\mathrm{d}y = 4000$), enriched with primary hyperons at mid-rapidity ($|y| < 1$):

- 100 $\Lambda + 100\ \overline{\Lambda}$;
- 15 $\Xi^- + 15\ \overline{\Xi}^+$.

For the Λ reconstruction, we use the set of topological selections described in Table 6. The corresponding average number of reconstructed Λ candidates (i.e. including background) is 6.6 per event with a purity of 85% in the invariant mass window $[1115.7 \pm 5]$ MeV/c^2.

b_-	b_+	DCA	$\cos\Theta$
0.15	0.10	0.10	0.9997

Table 6: Selections used for the Λ reconstruction (same variable definitions as in Section 1.2).

The resonant H^0 reconstruction procedure is a simple algorithm that associates all the pairs of Λ candidates within an event. Therefore, in order to increase the statistics, we choose the strategy to generate lighter ('fast') events, each of them containing only Λ and H^0 particles: after reconstruction with the set of selections given in Table 6, we obtain the same number of Λ candidates in the defined mass window as for realistic ones (i.e. 6.6 per event). In this way, we create approximately the same conditions as for full real events: the number of correlations between two Λ candidates must be the same, and we significantly decrease memory space and time consumption for this study.

In the 'fast' simulation, both Λ and H^0 are generated according to an exponential p_T distribution. The chosen physical properties of the simulated H^0 are consistent with a resonance and are presented below:

- mass: $m_{\mathrm{H^0}} = 2252$ MeV/c^2;
- branching ratio of $\mathrm{H^0} \to \Lambda\Lambda$: 100%;
- width: $\Gamma_{\mathrm{H^0}} = 13$ MeV/c^2.

A total of 10k 'fast' events were generated, each containing 110 Λ and 5 $\mathrm{H^0}$, and used to estimate both the $\mathrm{H^0}$ recontruction rate (for signal) and the background level coming from primary Λ candidates. The average number of reconstructed primary Λ candidates per event is 6.7, which is close to the expected 6.6.

The $\mathrm{H^0}$ reconstruction rate obtained with the 'fast' simulation is $7 \cdot 10^{-2}$%. The invariant mass spectra of the reconstructed Monte Carlo $\mathrm{H^0}$ are shown on Fig. 19 with (left panel) and without (right panel) the combinatorial background. It should be noted that the combinatorial background has been computed without any contribution from the $\mathrm{H^0}$ daughter particles. This is based on the assumption that the contribution of correlated background (for instance the correlation between a Λ daughter from an $\mathrm{H^0}$ and a primary Λ) is insignificant due to the low expected production yields for the $\mathrm{H^0}$.

We obtain a signal which is hardly discernable from the background. This significance gets worse as the $\mathrm{H^0}$ width is increased.

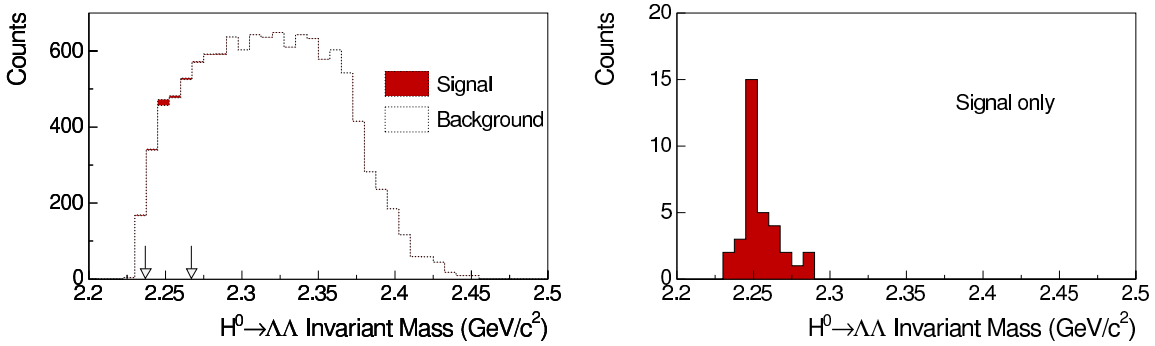

Figure 19: Left panel: Invariant mass of reconstructed Monte Carlo $\mathrm{H^0}$ and background coming from non-$\mathrm{H^0}$ daughters. Right panel: Invariant mass of reconstructed Monte Carlo $\mathrm{H^0}$ only.

The $\mathrm{H^0}$ reconstruction rate and background level obtained with these 10k events provide an estimate of the 3-σ sensitivity for such a particle, as was done previously for the weak decays, defining here the significance in the mass range 2252 ± 15 MeV/c^2. Hence, to get a 3-σ significance peak within a statistics of 10^7 events, the production yield of $\mathrm{H^0}$, in the interval $-1 < y < 1$, must be at least 0.74, or $\mathrm{d}N_{\mathrm{H^0}}/\mathrm{d}y = 0.37$, assuming a flat rapidity distribution.

2.7 Discussion on strange dibaryons

The studies performed in this section and the stated sensitivity estimations rely on several hypotheses chosen for the simulation. Parameters like mass, inverse slope, branching ratio or lifetime of the considered dibaryons are not precisely known, although some theoretical

estimations exist [27]. Different values would affect the reconstruction rates, and therefore the sensitivities. Nevertheless, the simulation parameters were chosen within reasonable limits of the predictions, and the given estimations of sensitivity, which are not claimed to be exact, represent the order of magnitude of ALICE's capabilities to identify such particles.

References

[1] A. Andronic, P. Braun-Munzinger, and J. Stachel, (2005), nucl-th/0511071.

[2] STAR, J. Adams *et al.*, Nucl. Phys. **A757**, 102 (2005), nucl-ex/0501009.

[3] P. Braun-Munzinger, J. Cleymans, H. Oeschler, and K. Redlich, Nucl. Phys. **A697**, 902 (2002), hep-ph/0106066.

[4] J. Rafelski and J. Letessier, J. Phys. **G30**, S1 (2004), hep-ph/0305284.

[5] J. Rafelski and B. Muller, Phys. Rev. Lett. **48**, 1066 (1982).

[6] NA57, G. E. Bruno, J. Phys. **G30**, S717 (2004), nucl-ex/0403036.

[7] STAR, H. Caines, J. Phys. **G31**, S1057 (2005), nucl-ex/0412015.

[8] A. Tounsi and K. Redlich, (2001), hep-ph/0111159.

[9] H. van Hecke, H. Sorge, and N. Xu, Phys. Rev. Lett. **81**, 5764 (1998), nucl-th/9804035.

[10] STAR, J. Adams *et al.*, (2006), nucl-ex/0601042.

[11] STAR, M. Heinz, J. Phys. **G31**, S141 (2005), hep-ex/0501017.

[12] X.-N. Wang and M. Gyulassy, Phys. Rev. **D44**, 3501 (1991).

[13] X.-N. Wang and M. Gyulassy, Phys. Rev. **D45**, 844 (1992).

[14] M. Gyulassy and X.-N. Wang, Comput. Phys. Commun. **83**, 307 (1994), nucl-th/9502021.

[15] Y. Kluger, V. Koch, J. Randrup, and X.-N. Wang, Phys. Rev. **C57**, 280 (1998), nucl-th/9704018.

[16] X.-N. Wang, Nucl. Phys. **A661**, 609 (1999), nucl-th/9907093.

[17] STAR, J. Adams *et al.*, Phys. Rev. Lett. **92**, 182301 (2004), nucl-ex/0307024.

[18] STAR, C. Adler *et al.*, Phys. Rev. Lett. **89**, 092301 (2002), nucl-ex/0203016.

[19] PHENIX, K. Adcox *et al.*, Phys. Rev. Lett. **89**, 092302 (2002), nucl-ex/0204007.

[20] ALICE, CERN-LHCC-95-71.

[21] A. Andronic and P. Braun-Munzinger, Lect. Notes Phys. **652**, 35 (2004), hep-ph/0402291.

[22] STAR, R. Witt, J. Phys. **G31**, S863 (2005).

[23] STAR, J. Adams *et al.*, Phys. Rev. Lett. **92**, 052302 (2004), nucl-ex/0306007.

[24] R. L. Jaffe, Phys. Rev. Lett. **38**, 195 (1977).

[25] J. F. Donoghue, E. Golowich, and B. R. Holstein, Phys. Rev. **D34**, 3434 (1986).

[26] S. D. Paganis *et al.*, Phys. Rev. **C62**, 024906 (2000), nucl-ex/9910007.

[27] J. Schaffner-Bielich, R. Mattiello, and H. Sorge, Phys. Rev. Lett. **84**, 4305 (2000), nucl-th/9908043.

[28] H. Sorge, M. Berenguer, H. Stoecker, and W. Greiner, Phys. Lett. **B289**, 6 (1992).

[29] H. Sorge, Phys. Rev. **C52**, 3291 (1995), nucl-th/9509007.

[30] H. Takahashi *et al.*, Phys. Rev. Lett. **87**, 212502 (2001).